UCRL-17434

University of California

Ernest O. Lawrence Radiation Laboratory

MATCHING AND BACKING PROBLEMS IN PIEZOELECTRIC READOUT SYSTEMS

Berkeley, California

DISCLAIMER

Submitted to Nuclear Instruments
and Methods

UCRL-17434
Preprint

(pages 8 & 9 corrected)

UNIVERSITY OF CALIFORNIA

Lawrence Radiation Laboratory
Berkeley, California

AEC Contract No. W-7405-eng-48

MATCHING AND BACKING PROBLEMS IN PIEZOELECTRIC READOUT SYSTEMS

Branko Leskovar

March 16, 1967

MATCHING AND BACKING PROBLEMS IN PIEZOELECTRIC READOUT SYSTEMS*

Branko Leskovar

Lawrence Radiation Laboratory
University of California
Berkeley, California

March 16, 1967

ABSTRACT

The effects of matching and backing on the performance of the piezoelectric ceramic transducers used in delay line readout systems for spark chambers are considered. Analysis and probe design are presented for a nonresonant matching system intended for pulse-strain detection application. Particular emphasis is laid on determination of the input acoustical impedance of an exponential matching connector. The input acoustical impedance is calculated and plotted as a function of (a) the normalized frequency, (b) the specific acoustical impedances ratio between the backing material and the matching connector material, and (c) the ratio of the large end diameter-to-small end diameter of the connector.

*Work done under the auspices of the U. S. Atomic Energy Commission.

Introduction

In wire spark chambers with delay line readout systems, the spark position is determined by the arrival time of a pulse generated by the spark at a suitably situated detector. From a number of proposed delay line methods[1, 2], most systems use the magnetostrictive effect[3-5]; with this method a pulse of magnetic field produces a local mechanical stress in a ferromagnetic wire which propagates as an ultrasonic stress pulse along the delay-line wire toward a receiving transducer. The transducer is usually a magnetically biased coil in which output pulses are produced by the change in magnetization of the wire element due to the strain wave at the place of the transducer[4]. The magnetostrictive effect exploited at generation of ultrasonic stress pulse, and the inverse magnetostrictive effect used at the receiving transducer, strongly depend upon density of the magnetic flux in the wire. Amplitude of the ultrasonic stress pulse at its generation decreases with magnetic saturation of the delay line wire. At the receiving transducer, the output pulse has a maximum value for an optimum amount of the magnetic bias. Output pulse amplitude generally decreases with any change in the magnetic bias from its optimum value. Influence of an ambient magnetic field can be reduced by orienting the delay line wire at right angles to the field direction, and by using a long delay line in an experimental arrangement where spark chambers need to be located in a magnetic field[6]. Since the receiving transducer is very sensitive to a high magnetic field, it is necessary for the transducer to be located in a fringing field no greater than 2 kG. Below this value, effective transducer magnetic shielding can be accomplished. A long delay line can be employed between the spark chamber and the shielded transducer.

A piezoelectric receiving transducer, which is essentially unaffected by magnetic fields, was tried out in an experimental set-up[6]. It produced larger output signals than the magnetically biased coil, but large acoustical impedance mismatching at two interfaces--between the delay line and the transducer, and between the transducer and the absorbing backing--produced reflections and broadened the output pulse.

Generally, the acoustical impedance mismatching is larger at the interface of the delay line wire end and the transducer than at the interface of the transducer and the absorbing backing. Consequently, the acoustical impedance mismatching of the first interface has a major influence on reflections. This is because the diameter of commercially available transducers is larger than the allowable diameter of the wire used as a delay line. The most common form of wave propagation used in delay line wire for readout applications is the longitudinal mode. However, the first longitudinal mode of wave propagation in wire is slightly dispersive when the wire diameter is a small fraction of the wavelength. In practical applications the wire diameter should be approximately 0.1 mm for equivalent operating frequency in the low megahertz range. Available thicknesses of commercially manufactured piezoelectric transducers have diameters of approximately 3 mm. From the standpoint of technical feasibility, the lower limit of the transducer minimum diameter is approximately 1.0 mm. Accordingly, in the best case, the acoustical impedance ratio between the delay line wire and the transducer at their interface is approximately 100, even when the wire material and the transducer material have equal specific acoustical impedances. Furthermore, the ultrasonic stress pulse will be distributed

very non-uniformly over the receiving transducer input surface when the delay line wire and the receiving transducer are in direct contact over only a relatively small area of the delay line wire. Both effects--the abrupt change in acoustical impedances at the interface of wire end and the transducer, and non-uniform distribution of stress pulse over the transducer surface--will have such very undesirable consequences as reflections of ultrasonic energy from the transducer input face, transducer resonances, and distortion of the output pulse. For these reasons, it is important to insert a connector with a gradually increasing cross-sectional area between the delay line wire end and the receiving transducer input face. The most advantageous connector so far employed in physical acoustics is the exponential connector, the purpose of which is to transform the transducer acoustical impedance to the delay line wire acoustical impedance.

The purpose of this paper is to obtain useful applicable results for designing a readout receiving probe, when semi-matched conditions of acoustical impedances are fulfilled. These results were derived from basic acoustical properties of the experimental and the cylindrical connectors.

Input acoustical impedance of the exponential connector

In designing the exponential connector for the previously mentioned application, we selected the connector parameters so that the connector transfers the maximum amount of ultrasonic energy into a piezoelectric transducer over the desired frequency range with minimum internal reflections, resonances, and distortions. Although a complete analysis of the ultrasonic stress-wave motion in a solid, finite-length, exponential connector used in a receiving probe configuration is very

complicated, one can use an approximate method of calculation and obtain fairly satisfactory results if the connector is many wavelengths long. For an exponential connector in the probe configuration shown in Fig. 1, the cross-sectional area at any point along its length is given by the expression

$$A_x = A_i \exp (m_o x) , \tag{1}$$

where A_x is the cross-sectional area (in metre^2) at point x along the connector axis, A_i is the cross-sectional area of the small end of the connector (in this consideration, it is equal to the cross-sectional area of the wire used as a delay line), m_o is the flare constant in metre^{-1}, and x is the distance from the connector's smaller end in metre. The flare constant m_o determines the rapidity of the flare; the greater m_o is, the greater is the curvature of the connector. For an exponential connector of finite length, which is the case in the present application, the modified approximate expression for the input acoustical impedance in kg/m^4 sec according to Olson[7] is

$$Z_i = \frac{\rho v}{A_i} \frac{A_o Z_o \cos (bl + \theta) + j\rho v \sin bl}{jA_o Z_o \sin bl + \rho v \cos (bl - \theta)} , \tag{2}$$

where ρ is the density of the connector material in kg/m^3, v is the velocity of ultrasonic wave propagation in m/sec, Z_o is the acoustical impedance of the backing material in kg/m^4 sec, and l is the total connector length in metre. Other terms are defined by the following equations:

$$\theta = \tan^{-1} (m_o/2b) \tag{3}$$

$$b = \tfrac{1}{2} (4p^2 - m_o^2)^{1/2} \tag{4}$$

$$p = 2\pi/\lambda , \tag{5}$$

where λ is the wavelength in metre. The flare constant is given by

$$m_o = 4\pi f_c / v, \tag{6}$$

where f_c is the connector cutoff frequency in hertz units. From further considerations it will be seen that there is generally a sudden change in the input acoustical impedance of a finite-length connector in the frequency region around the cutoff frequency.

If the connector is coupled to a long circular backing rod of area A_o, made of a material with the specific acoustical impedance $\rho_o v_o$ (where ρ_o is the rod's material density, and v_o is the velocity of propagation of an ultrasonic wave in rod), one can substitute the expression for a circular rod acoustical impedance

$$Z_o = \rho_o v_o / A_o \tag{7}$$

into equation (2) and rewrite equation (2) to express the acoustical impedance in a normalized form

$$Z_i \frac{A_i}{\rho v} = \frac{K \cos (bl + \theta) + j \sin bl}{\cos (bl - \theta) + jK \sin bl}, \tag{8}$$

where the matching factor K is defined as a ratio between the specific acoustical impedance of the backing rod material and the connector material

$$K = \rho_o v_o / \rho v. \tag{9}$$

From equation (8) can be seen that the normalized acoustical impedance of a finite exponential connector basically consists of a real part and an imaginary part

$$Z_i \frac{A_i}{\rho v} = \mathrm{Re}\left(Z_i \frac{A_i}{\rho v} \right) + \mathrm{Im}\left(Z_i \frac{A_i}{\rho v} \right). \tag{10}$$

The actual amount of the real and the imaginary parts of the connector input acoustical impedance, or the acoustical resistance and the acoustical reactance, respectively, can be calculated from this equation

for a particular set of parameters. The connector input acoustical resistance and reactance as a function of the frequency, the connector geometrical dimensions, and the specific acoustical impedance of the connector material and the backing rod material are very important in determining the optimum connector dimensions and the readout receiving probe configuration. From the standpoint of a minimum reflection at the interface of the end of the delay line wire and the smaller end of the connector, and a transmission of ultrasonic energy from the wire's end of the piezoelectric transducer, the amount of the acoustical resistance needs to be maximized with respect to the acoustical reactance in a given frequency range of interest. For this purpose, the input acoustical resistance and reactance expressions are derived from equation (8) as a function of the normalized frequency, the ratio D_o/D_i of the diameters of the large end to the small end of the connector, and the specific acoustical impedance ratio K between the backing material and the matching connector material.

Because the exponential connector shows (a) a larger ratio of the acoustical resistance to the acoustical reactance and (b) more uniform acoustical resistance characteristics over a frequency range for a finite dimension of connector than other types of connectors (e.g. parabolic, conical, or hyperbolic), only the exponential one will be considered. The properties of cylindrical types will be determined as a special case of the exponential connector.

Acoustical resistance and reactance expressions for solid exponential and cylindrical connectors

The readout receiving probe consists of a solid exponential connector and various cylindrical components. Input acoustical resistance and reactance of exponential and cylindrical components can be derived directly from equation (2). For this purpose the terms bl and θ in equation (2) have to be represented as a function of normalized frequency and the diameter ratio, D_o/D_i, of the connector. Using equations (1), (3), (4), (5), and (6), we obtain

$$bl = \left[(f/f_c)^2 - 1 \right]^{1/2} \log_\epsilon (D_o/D_i) \tag{11}$$

and

$$\theta = \tan^{-1} \frac{1}{\left[(f/f_c)^2 - 1 \right]^{1/2}} . \tag{12}$$

The following interesting cases can be directly derived with equations (2), (11), and (12).

1. When $f < f_c$, or below the frequency corresponding to bl = 0, the terms bl and θ will be imaginary, and the following equations will be valid:

$$bl = j \left| \left[(f/f_c)^2 - 1 \right]^{1/2} \log_\epsilon (D_o/D_i) \right| \tag{13}$$

and

$$\theta = \tan^{-1} \left\{ -j \left| \frac{1}{(f/f_c)^2 - 1} \right|^{1/2} \right\} . \tag{14}$$

When the following equations[8] are employed

$$\tan^{-1} (-jy) = \frac{j}{2} \log_\epsilon \frac{1 - y}{1 + y} \tag{15}$$

and

$$\log_\epsilon (-1) = \pm j\pi (2K^* + 1) , \tag{16}$$

where K^* is any integer--the term θ can be expressed by the relation

$$\theta = \pm \frac{\pi}{2} + \frac{j}{2} \log_\epsilon \left| \frac{1 - y}{1 + y} \right| \tag{17}$$

where

$$y = \left[\left| \frac{1}{(f/f_c)^2 - 1} \right| \right]^{1/2} . \tag{18}$$

Furthermore, by means of equations

$$\sin jx = j \sin hx \tag{19}$$

and

$$\cos (a + jb) = \cos a \cos hb - j a \sin hb, \text{ ina} \tag{20}$$

the connector input acoustical resistance and reactance can be calculated.

They are given by the expressions

$$\mathrm{Re}\left(Z_i \frac{A_i}{\rho v} \right) = K \frac{\sin h^2 x - \sin h(x + \frac{1}{2} \log_\epsilon u) \sin h(x - \frac{1}{2} \log_\epsilon u)}{K^2 \sin h^2 x + \sin h^2 (x - \frac{1}{2} \log_\epsilon u)} \tag{21}$$

and

$$\mathrm{Im}\left(Z_i \frac{A_i}{\rho v} \right) = j \sin hx \frac{\pm \sin h (x - \frac{1}{2} \log_\epsilon u) \pm K^2 \sin h(x + \frac{1}{2} \log_\epsilon u)}{K^2 \sin h^2 x + \sin h^2 (x - \frac{1}{2} \log_\epsilon u)} \tag{22}$$

where x and u are given by the equations

$$x = \left| [(f/f_c)^2 - 1] \right|^{1/2} \log_\epsilon (D_o/D_i) \tag{23}$$

$$u = \frac{1 - y}{1 + y} . \tag{24}$$

2. When $f = f_c$, or $4K^2 = m_o^2$, equation (8) is indeterminate. Making the derivation of numerator and denominator with respect to b, and setting b equal to 0 give an evaluated expression for the input acoustical impedance:

$$Z_i \frac{A_i}{\rho v} = \frac{K[1 - \log (D_o/D_i)] + j \log_\epsilon (D_o/D_i)}{1 + \log_\epsilon (D_o/D_i) + jK \log_\epsilon (D_o/D_i)} . \tag{25}$$

From equation (25) the normalized input acoustical resistance and reactance of the connector can be expressed by the relations

$$\mathrm{Re}\left(Z_i \frac{A_i}{\rho v}\right) = \frac{K}{\left[1 + \log_\epsilon (D_o/D_i)\right]^2 + K^2 \left[\log_\epsilon (D_o/D_i)\right]^2} \tag{26}$$

$$\mathrm{Im}\left(Z_i \frac{A_i}{\rho v}\right) = j \frac{\log_\epsilon (D_o/D_i)\left[1 + \log_\epsilon (D_o/D_i)\right] - K^2 \log_\epsilon (D_o/D_i)\left[1 - \log_\epsilon (D_o/D_i)\right]}{\left[1 + \log_\epsilon (D_o/D_i)\right]^2 + K^2 \left[\log_\epsilon (D_o/D_i)\right]^2} \tag{27}$$

respectively.

3. When $f > f_c$, the normalized connector input acoustical resistance and reactance can be directly calculated from equation (8). Such calculation gives

$$\mathrm{Re}\left(Z_i \frac{A_i}{\rho v}\right) = K \frac{\cos (bl + \theta) \cos (bl - \theta) + \sin^2 bl}{\cos^2 (bl - \theta) + K^2 \sin^2 bl} \tag{28}$$

$$\mathrm{Im}\left(Z_i \frac{A_i}{\rho v}\right) = j \sin bl \frac{\cos (bl - \theta) - K^2 \cos (bl + \theta)}{\cos^2 (bl - \theta) + K^2 \sin^2 bl}, \tag{29}$$

where bl and θ are given by equations (11) and (12).

4. For $D_o/D_i = 1$, the exponential connector becomes the finite cylindrical connector. The flare constant m_o equals 0; consequently b equals $(4p^2 - m_o^2)^{1/2}/2$ equals p, and θ equals $\tan^{-1} m_o/2b$ equals 0. Using expressions (5) and $l = v/f_c$, we find that the term $pl = 2\pi f/f_c$. The normalized input acoustical resistance and reactance of cylindrical connector directly given from equation (8) are

$$\mathrm{Re}\left(Z_i \frac{A_i}{\rho v}\right) = \frac{K}{K^2 \sin^2 w + \cos^2 w} \tag{30}$$

$$\mathrm{Im}\left(Z_i \frac{A_i}{\rho v}\right) = j \frac{(1 - K^2) \sin w \cos w}{K^2 \sin^2 w + \cos^2 w}, \tag{31}$$

where w equals $2\pi f/f_c$.

By means of a digital computer, the exponential and the cylindrical connector input acoustical resistance and reactance as a function of the normalized frequency with the connector diameter ratio, D_o/D_i, and the matching factor, K, as parameters are calculated and plotted as shown in Figs. 2 - 26.

The normalized input acoustical resistance and reactance characteristics of the cylindrical connector as a function of the normalized frequency and other significant parameters are given in Figs. 2, 3, 9, 16, 20, and 21. These figures show that the variations in the input acoustical resistance and reactance as a function of normalized frequency are quite large in amplitude, even for a relatively small value of the acoustical impedance mismatch between the connector material and the backing material. For a perfect matching [when the matching factor $K = \rho_o v_o/\rho v = 1$, from equations (30) and (31)], it directly follows that the $\mathrm{Re}(Z_i A_i/\rho v)$ equals 1, and $\mathrm{Im}(Z_i A_i/\rho v)$ equals 0. For a matching factor of 0.8 or 1.2, the amplitude variations in acoustical resistance will be approximately ±20% of the normalized resistance value of 1. If the matching factor is 0.5 or 2.0, it can be seen from Figs. 2, 3, 20, and 21 that the acoustical resistance amplitude variation will be approximately +100% and -50% of the normalized resistance value. The acoustical reactance will vary around zero for approximately ±75% of the normalized resistance value.

For the exponential connector and with perfect matching, the acoustical resistance and reactance change suddenly in the frequency region around the normalized frequency point $f/f_c = 1$. An actual value of the acoustical resistance in the region below $f/f_c = 1$ depends strongly upon the connector diameter ratio, D_o/D_i. For a small D_o/D_i, the connector

input acoustical resistance will have an appreciable value below the normalized frequency $f/f_c = 1$, which means that the connector will transmit ultrasonic energy below this frequency. However, with increasing D_o/D_i, the acoustical resistance in this frequency region will be very small, and will prevent an efficient transmission of energy through the connector, as can be concluded by a comparison of the resistance characteristics given in Figs. 13, 14, and 15. In contrast, the acoustical reactance magnitude increases with increasing D_o/D_i in the same frequency region. For the most practical application, D_o/D_i is equal to or larger than 10, when the acoustical resistance below the point $f/f_c = 1$ has a small value. About the region of the cutoff frequency, the normalized acoustical resistance approaches unity. In contrast, the acoustical reactance approaches zero in both directions from the point $f/f_c = 1$.

When the matching factor is equal to 0.5, 0.8, 1.2, and 2.0, the acoustical resistance and reactance characteristics will generally have the same basic behaviour as in the cases just described for the region around the point $f/f_c = 1$, except that the first amplitude characteristics will be shifted along the f/f_c axis, as one can conclude from Figs. 4 – 8, 10 – 12, 17 – 19, and 22 – 26. Furthermore, the common property of the acoustical resistance characteristics is that they will never asymptotically approach the normalized unity value when f/f_c increases, as it did in the previous considerations for K = 1.0. In addition, the acoustical reactance characteristics will never approach zero as f/f_c increases. Both characteristics have amplitude variations of a constant magnitude for large f/f_c ratios on the right side of the point $f/f_c = 1$. The magnitude of amplitude variations depends upon the matching factor value; as any change in this factor from

K = 1.0 increases the magnitude of amplitude variations. This effect can be easily seen by comparing Figs. 11 and 18 with Figs. 5, 6, 23, and 24. Meanwhile, the separation between the successive maxima of amplitude variations is increased as D_o/D_i increases.

Readout-probe design considerations

The connector's acoustical characteristics can now be used for determination of its optimum length, the readout-probe configuration, and the acoustical impedances of various probe elements. The main readout probe characteristics desired are a wide bandwidth and a low transmission loss which gives good sensitivity. A basic delay line readout probe configuration is shown in Fig. 1. A delay line wire of a specific acoustical impedance Z_D is soldered on the exponential connector's small end. The connector is made of a material with a specific impedance Z_E. A piezoelectric ceramic transducer, of a specific impedance Z_T, is joined to the larger end of the exponential connector and to the absorbing backing rod by means of indium solder or silver epoxy adhesive bonds of specific impedances Z_{B2} and Z_{B3}, respectively. The absorbing backing rod increases the readout probe bandwidth and absorbs the energy transmitted into the backing material to prevent false echoes.

The mutual dependence between the connector's total length, l, the connector's cutoff frequency, f_c, and the connector's diameter ratio, D_o/D_i, can easily be found by considering relations (1) and (6). If the area of the connector's larger end A_o and smaller end A_i are expressed by means of diameters D_o and D_i, on the basis of equations (1) and (6) an exponential connector length times cutoff frequency characteristic in metre · Hz can be expressed by the equation

$$lf_c = \frac{v}{2\pi} \log_e \frac{D_o}{D_i} , \qquad (32)$$

where v is the velocity of ultrasonic wave propagation in the connector material.

Graphical representation of this equation is shown in Fig. 27. By means of equation (32) the product of the connector length and cutoff frequency can be calculated, using the velocity of wave propagation in the connector material, the delay line wire diameter D_i, and the piezoelectric transducer parameter D_o. For maximum acoustical energy transmission through the connector, the connector cutoff frequency must be placed below the low-frequency limit of the frequency range.

Because the matching factor has an appreciable effect on the connector acoustical characteristics and consequently on the transmission of ultrasonic energy through the connector, the specific acoustical impedances of the delay line wire material, the connector material, the transducer material, and the backing rod material need to have identical values. In practice, it is very difficult to achieve matching factors > 0.8 and < 1.2 between the various readout probe components.

Between the end of the delay line wire and the smaller end of the connector, an adhesive bond with specific impedance Z_{B1} is unavoidable. The adhesive bonds of a finite length are also present between the connector's larger end and the transducer as well as between the transducer and the absorbing backing rod. These bonds will introduce some losses and reflections. The bonds' thickness must be minimized to reduce these undesirable effects.

On the basis of these considerations, a piezoelectric readout probe assembly for a spark chamber was designed. This assembly, shown in Fig. 28, consists of the components listed below with their impedances.

Component	Approximate material specific acoustical impedance (kg/m^2 sec)
Vacoflux delay line wire	47×10^6
Stainless steel exponential connector	40×10^6
Piezoelectric ceramic transducer PZT-5A	34×10^6
Absorbing backing lead rod	28×10^6

With a chosen connector cutoff frequency of 100 kHz, the required connector length is 25.4×10^{-3} m. The connector flare constant of $m_o = 2.52 \times 10^2 m^{-1}$ was calculated from equation (6) using the propagation velocity of a strain wave $v = 4990$ m/sec for nonmagnetic stainless steel. The vacoflux delay line wire was soldered on the connector's small end. The piezoelectric ceramic transducer was joined to the connector's larger end and to the absorbing backing rod by means of indium solder. Equally good results were achieved by using bubble-free layers of silver epoxy (E-solder No. 302 produced by Epoxy Products, Irvington, New Jersey) on both sides. The grounded side of the transducer is the one which is joined to the connector's larger end, and the other electrical connection is made by means of the backing lead rod. The complete probe assembly is shielded with a copper cylinder, at the end of which a miniature electrical connector is attached.

When an ultrasonic stress wave traverses the piezoelectric transducer, a potential difference is created by charge displacement between the opposite faces of the transducer. Figure 29 shows a typical output

signal and residual effects obtained from the readout probe assembly shown in Fig. 28. The horizontal scale is 0.5 μsec/division; the vertical scale is 100 mV/division. The output signal was obtained as a response to a confined magnetic field pulse introduced on the delay line approximately 15 cm from the transducer. The magnetic field pulse was produced by the passage of a 1.5A current pulse 0.2 μsec wide through a 20-turn coil.

The probe output pulse is also followed by some rings. These rings are associated with lateral modes in the probe assembly, and with the residual reflections due to the matching factor $K \neq 1$, between the delay line wire, the transducer, and the absorbing backing rod. The magnitude of these rings was inversely proportional to the transducer radius and grew more pronounced with an increase in transducer radius and with the application of an ultrasonic stress pulse. With the air backing, as well as the various low impedance backings (such as plastics and epoxy with $Z_m \approx 3 \times 10^6$ kg/m^{2}sec), the main output pulse was followed with several rings of approximately the same magnitude as the main pulse, due to the large acoustical impedance mismatch between the transducer and backing medium.

We tried using a higher impedance absorbing backing with centrifuged mixture of epoxy resin and 2μ or less particle size tungsten powder; with this mixture had an impedance of the order of 10×10^6 kg/m^{2}sec and the response was improved with respect to the amplitude of the rings. The shortest output pulse with a minimum reflection has been obtained with higher impedance backings such as pure zinc ($Z_m \approx 27 \times 10^6$ kg/m^{2}sec) and pure lead ($Z_m \approx 28 \times 10^6$ kg/m^{2}sec). The lead backing was apparently slightly better than zinc with respect to reflections from the end of the rod attached to the electrical connector; this is due to the better absorption properties of lead.

Conclusions

The effects of matching and backing on the performance of the piezoelectric ceramic transducers used in delay line readout systems for spark chambers are considered. Expressions have been derived for the input acoustical resistance and reactance of the cylindrical and the exponential connector of a readout probe configuration as a function of the normalized frequency, the connector matching factor, and the ratio of the diameters of the larger end to smaller end of the connector. From these expressions, as well as from the other results of the analysis, several formulas are obtained for design of a non-resonant readout probe assembly intended for pulse strain detection when the semimatched conditions between the various readout probe components are fulfilled.

Acknowledgements

The author would like to express his appreciation to Dr. Victor Perez-Mendez for helpful discussions and stimulating comments in the course of this work, Esther Coleman for computer programming and numerical computation, and Dick A. Mack for manuscript reading and helpful suggestions. The technical assistance of Ronald L. Grove is gratefully acknowledged.

References

1. G. Charpak, Nucl. Instr. Methods 15, 318 (1962).

2. G. Bertsch, Nucl. Instr. Methods 34, 175 (1965).

3. G. Giannelli, Nucl. Instr. Methods 31, 29 (1964).

4. V. Perez-Mendez and J. Pfab, Nucl. Instr. Methods 33, 141 (1965).

5. S. Miyamoto, Nucl. Instr. Methods 35, 323 (1965).

6. L. Kaufman, V. Perez-Mendez, J. M. Pfab, IEEE Trans. Nucl. Sci., NS-13, No. 3, 578 (June 1966).

7. H. F. Olson, Acoustical Engineering, (D. Van Nostrand Company, Inc., New York 1957) 108.

8. H. B. Dwight, Tables of Integrals and Other Mathematical Data, (The MacMillan Company, 1961, New York) 168.

Figure Captions

Fig. 1 Basic delay line readout probe configuration. See text for explanation of A_i and A_x.

Fig. 2. Cylindrical connector acoustical resistance characteristic with K = 0.5 and D_o/D_i = 1.0 as parameters.

Fig. 3. Cylindrical connector acoustical reactance characteristic with K = 0.5 and D_o/D_i = 1.0 as parameters.

Fig. 4. Exponential connector acoustical impedance characteristics with K = 0.5 and D_o/D_i = 2 as parameters.

Fig. 5. Exponential connector acoustical resistance characteristic with K = 0.5 and D_o/D_i = 10 as parameters.

Fig. 6. Exponential connector acoustical reactance characteristic with K = 0.5 and D_o/D_i = 10 as parameters.

Fig. 7. Exponential connector acoustical resistance characteristic with K = 0.5 and D_o/D_i = 100 as parameters.

Fig. 8. Exponential connector acoustical reactance characteristic with K = 0.5 and D_o/D_i = 100 as parameters.

Fig. 9. Cylindrical connector acoustical impedance characteristics with K = 0.8 and D_o/D_i = 1.0 as parameters.

Fig. 10. Exponential connector acoustical impedance characteristics with K = 0.8 and D_o/D_i = 2 as parameters.

Fig. 11. Exponential connector acoustical impedance characteristics with K = 0.8 and D_o/D_i = 10 as parameters.

Fig. 12. Exponential connector acoustical impedance characteristics with K = 0.8 and D_o/D_i = 100 as parameters.

Fig. 13. Exponential connector acoustical impedance characteristics with K = 1.0 and D_o/D_i = 2 as parameters.

Fig. 14. Exponential connector acoustical impedance characteristics with K = 1.0 and D_o/D_i = 10 as parameters.

Fig. 15. Exponential connector acoustical impedance characteristics with K = 1.0 and D_o/D_i = 100 as parameters.

Fig. 16. Cylindrical connector acoustical impedance characteristics with K = 1.2 and D_o/D_i = 1.0 as parameters.

Fig. 17. Exponential connector acoustical impedance characteristics with K = 1.2 and D_o/D_i = 2.0 as parameters.

Fig. 18. Exponential connector acoustical impedance characteristics with K = 1.2 and D_o/D_i = 10 as parameters.

Fig. 19. Exponential connector acoustical impedance characteristics with K = 1.2 and D_o/D_i = 100 as parameters.

Fig. 20. Cylindrical connector acoustical resistance characteristic with K = 2.0 and D_o/D_i = 1.0 as parameters.

Fig. 21. Cylindrical connector acoustical reactance characteristic with K = 2.0 and D_o/D_i = 1.0 as parameters.

Fig. 22. Exponential connector acoustical impedance characteristics with K = 2.0 and D_o/D_i = 2.0 as parameters.

Fig. 23. Exponential connector acoustical resistance characteristic with K = 2.0 and D_o/D_i = 10 as parameters.

Fig. 24. Exponential connector acoustical reactance characteristic with K = 2.0 and D_o/D_i = 10 as parameters.

Fig. 25. Exponential connector acoustical resistance characteristic with K = 2.0 and D_o/D_i = 100 as parameters.

Fig. 26. Exponential connector acoustical reactance characteristic with K = 2.0 and D_o/D_i = 100 as parameters.

Fig. 27. Exponential connector length × cutoff frequency characteristics relating to the ratio of the diameter of the larger end of the connector to the diameter of the smaller end of the connector.

Fig. 28. Diagram of the readout probe assembly for a spark chamber.

Fig. 29. Typical readout probe output signal obtained with a 3-mm diameter transducer; the horizontal scale is 0.5 μsec/division. The vertical scale is 100 mV/division.

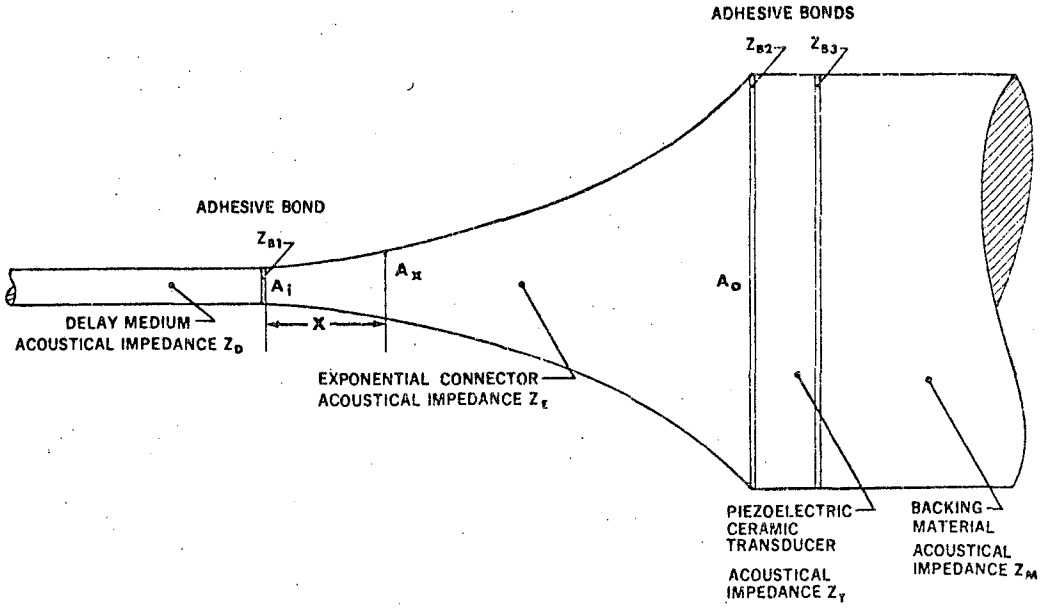

FIG 1

XBL 674-1339

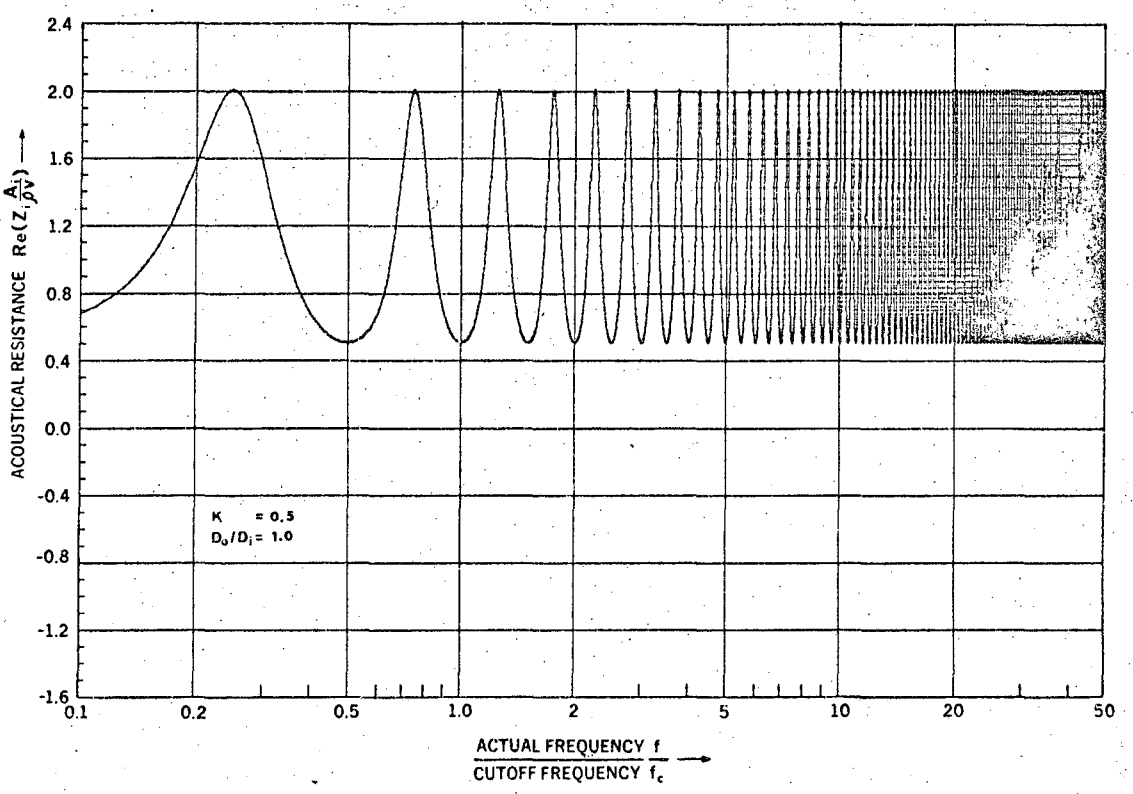

FIG. 2

XBL 674-1340

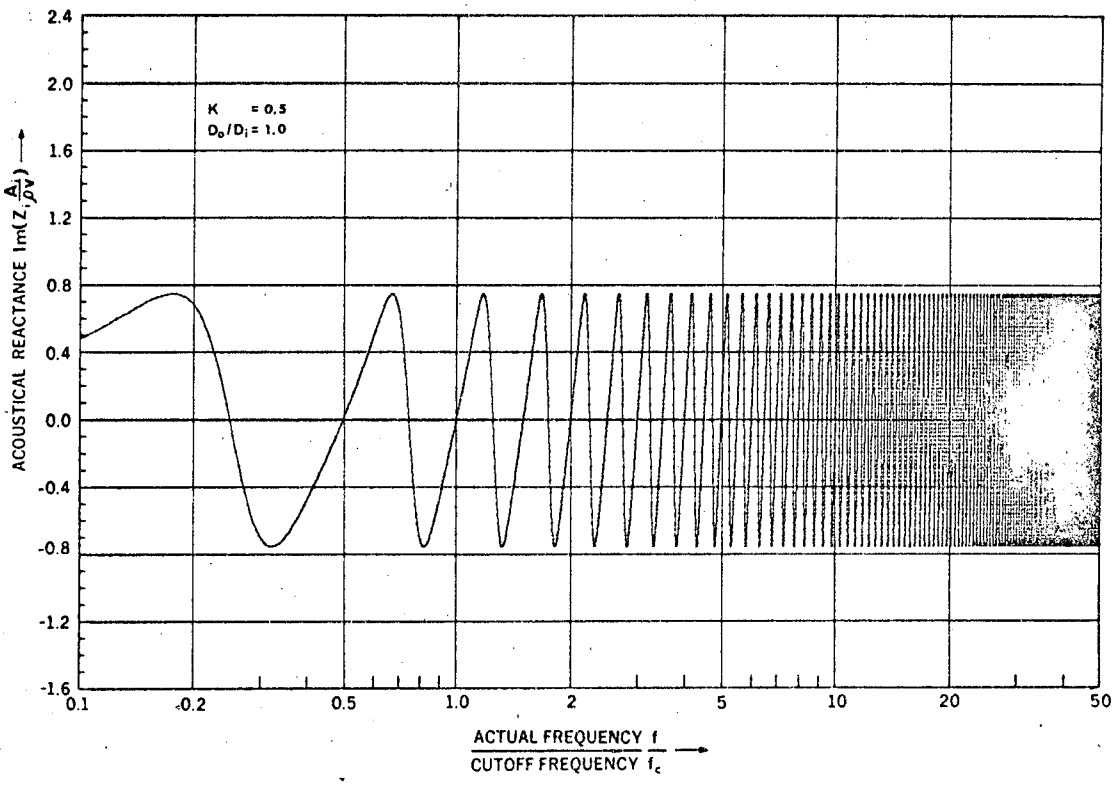

FIG. 3

XBL 674-1341

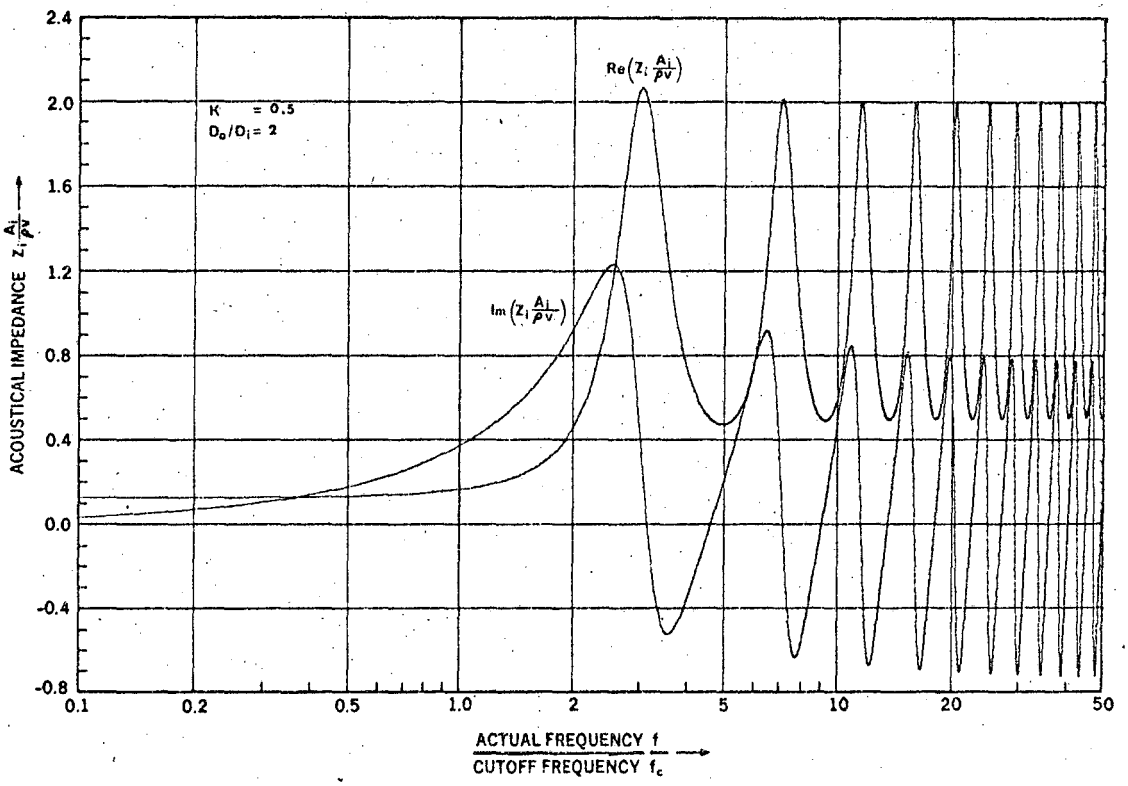

FIG. 4

XBL 674-1342

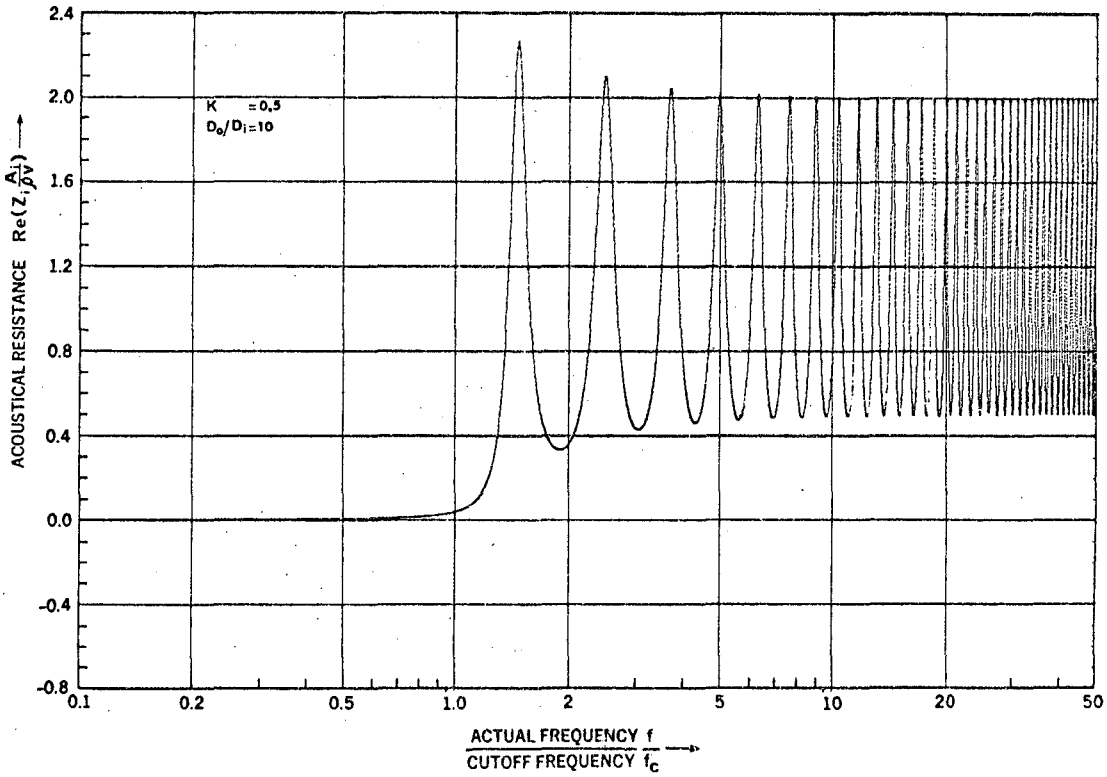

FIG. 5

XBL 674-1343

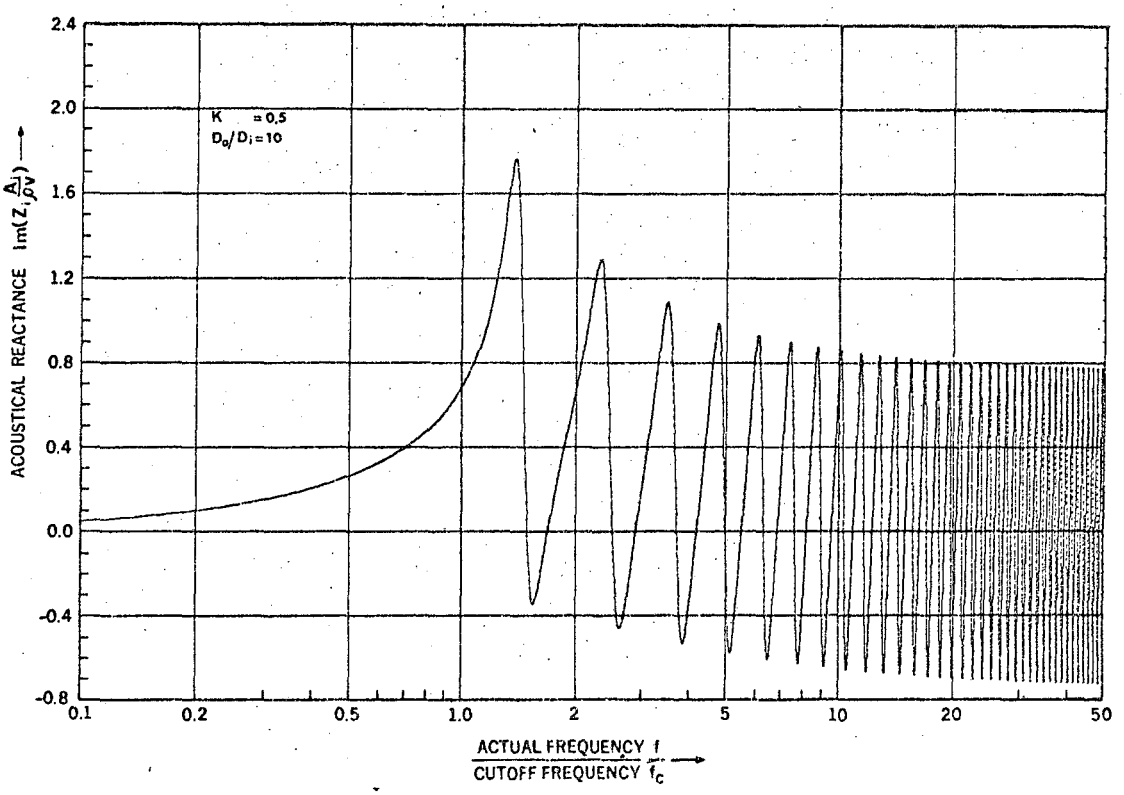

FIG. 6

XBL 674-1344

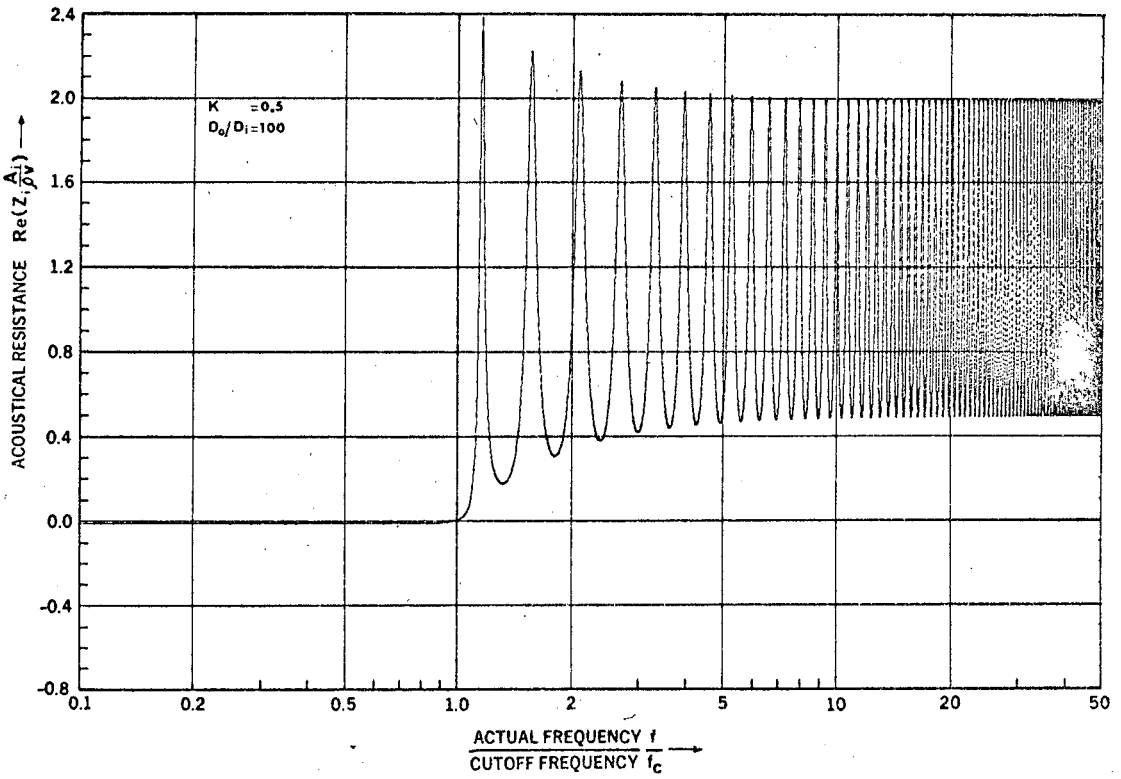

FIG. 7

XBL 674-1345

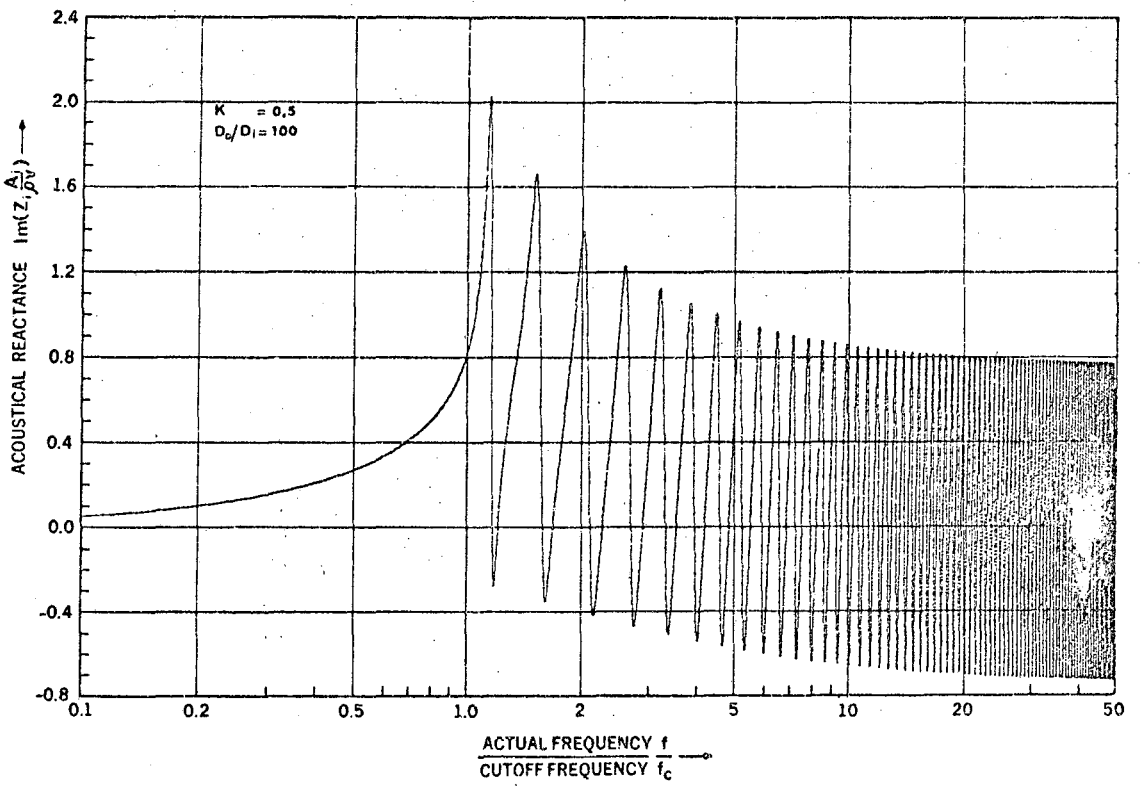

FIG. 8

XBL 674-1346

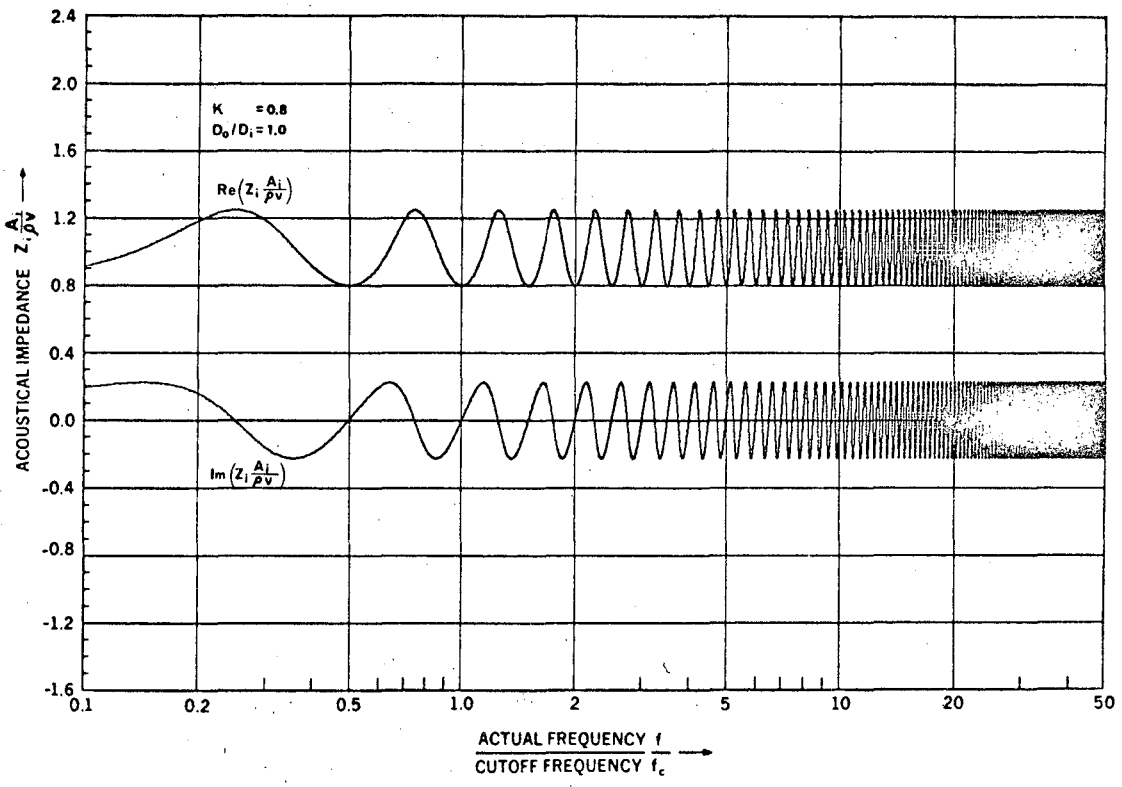

FIG. 9

XBL 674-1347

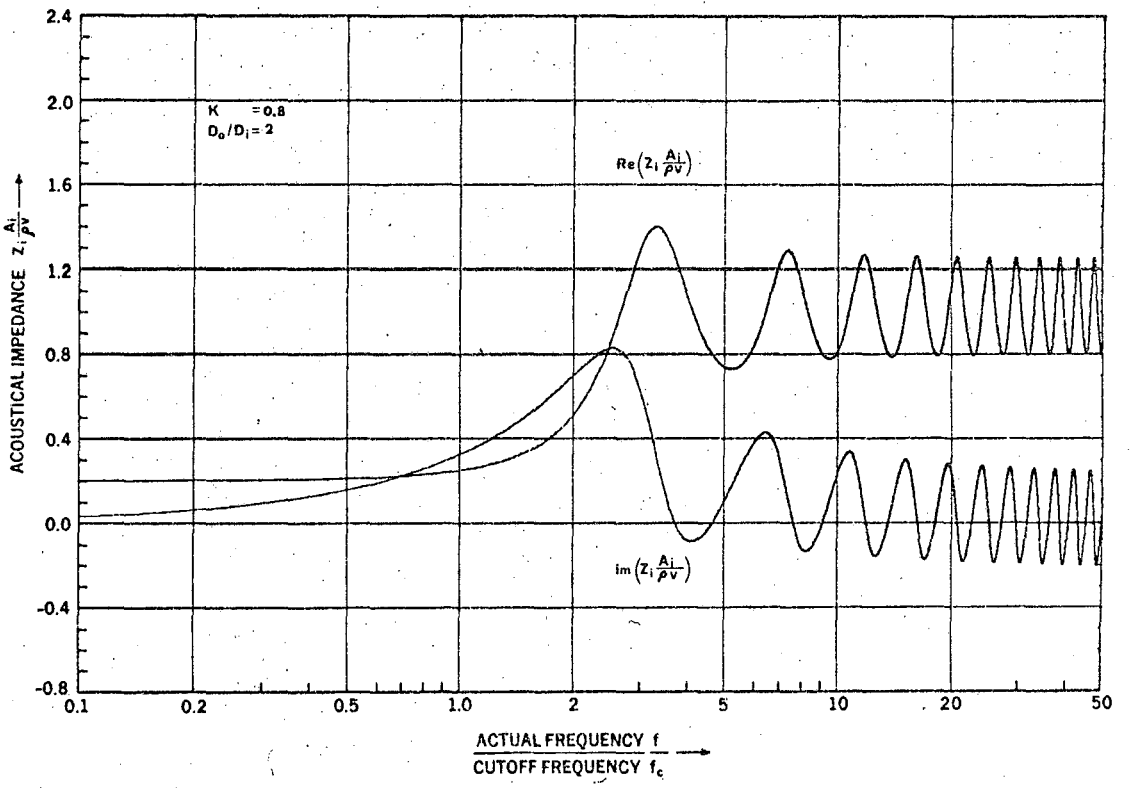

FIG. 10

XBL 674-1348

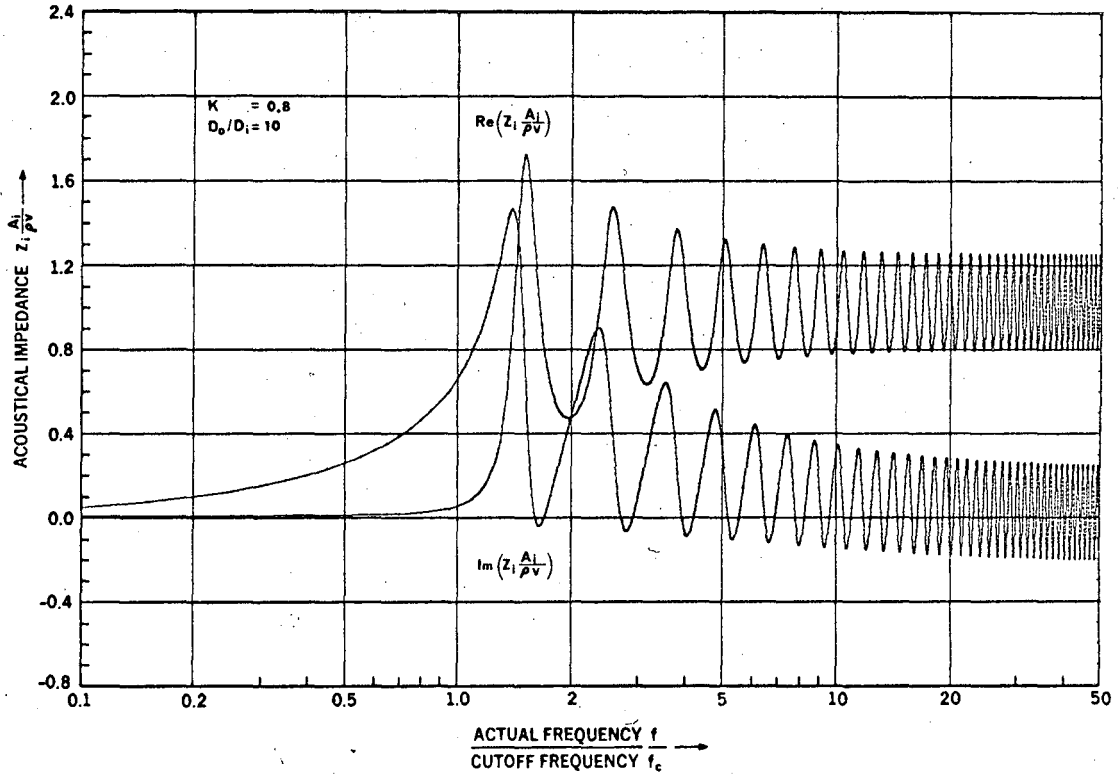

FIG. 11

XBL 674-1349

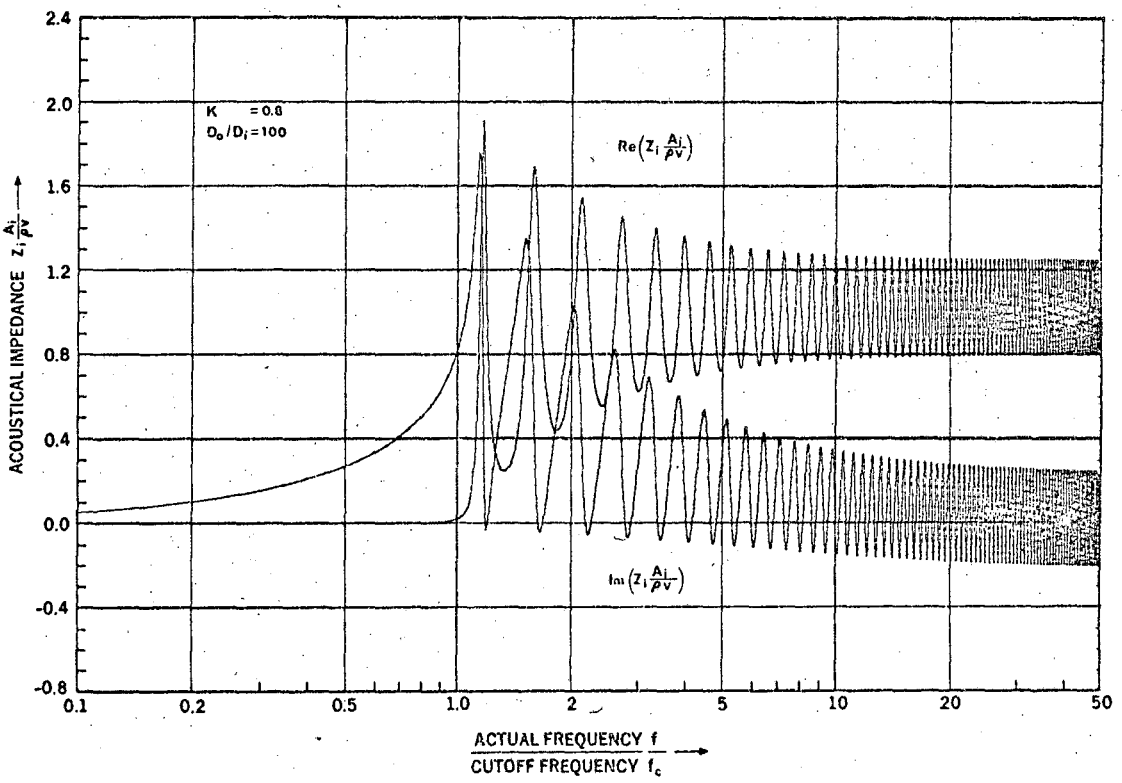

FIG. 12

XBL 674-1350

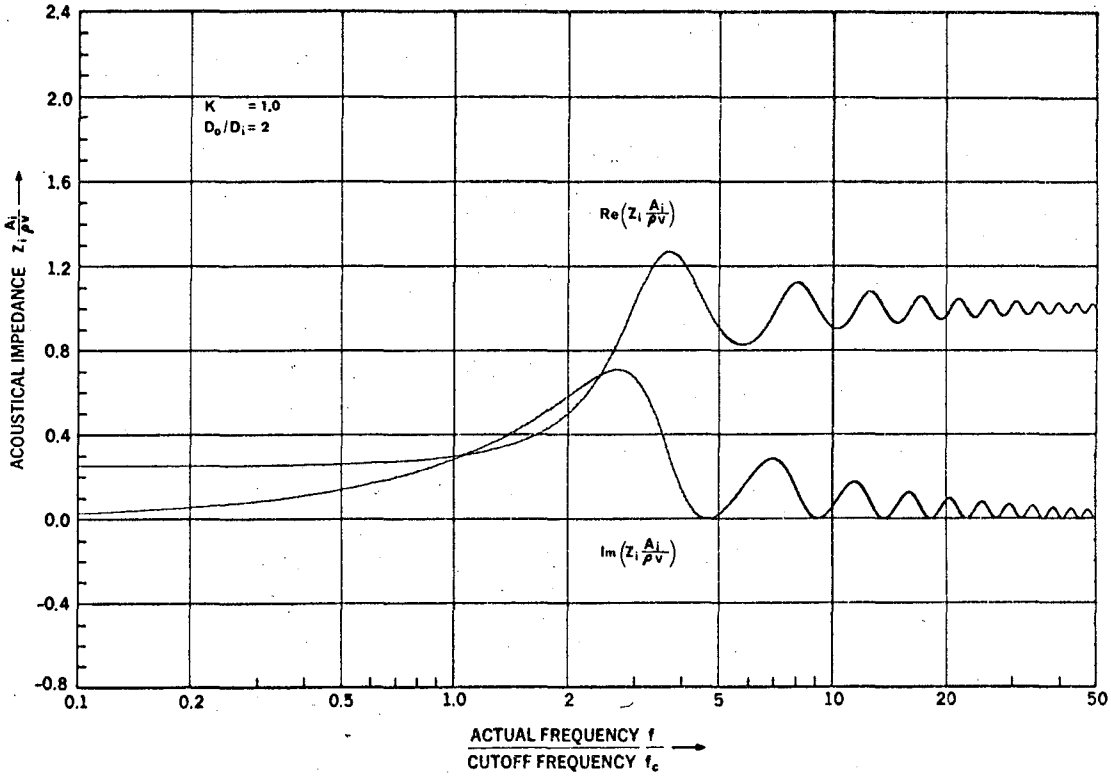

FIG. 13

XBL 674-1351

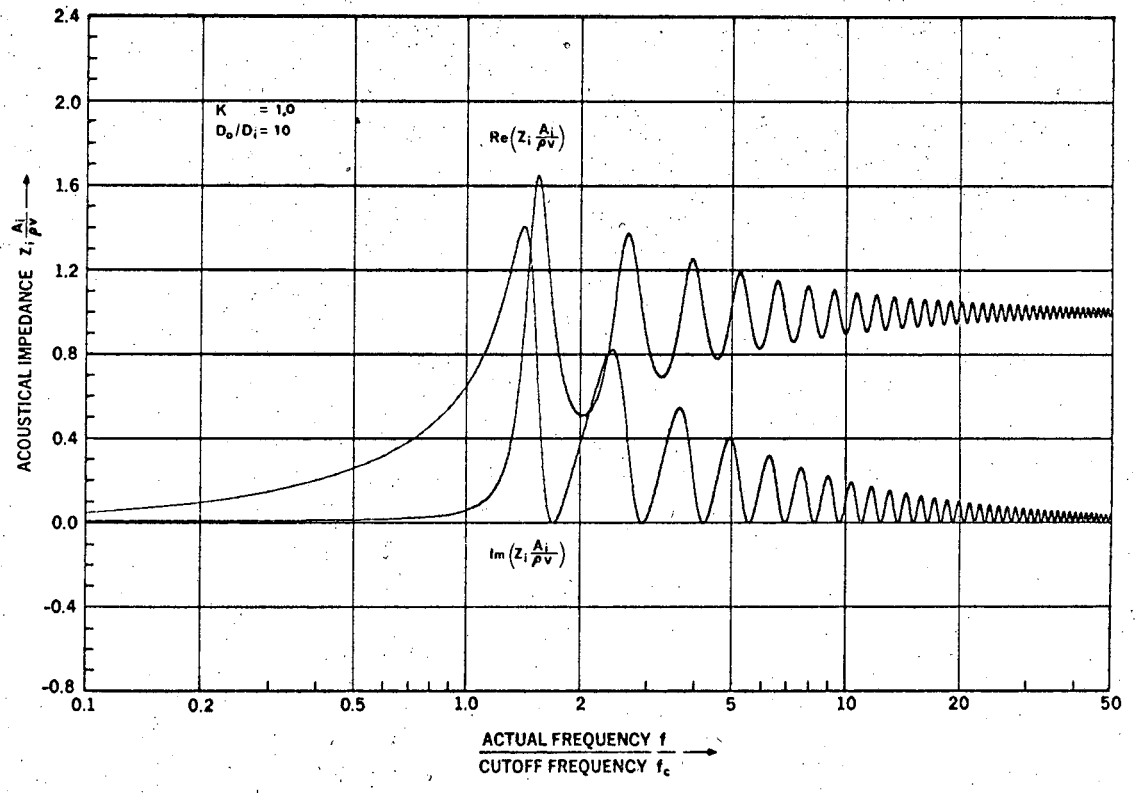

FIG. 14

XBL 674-1352

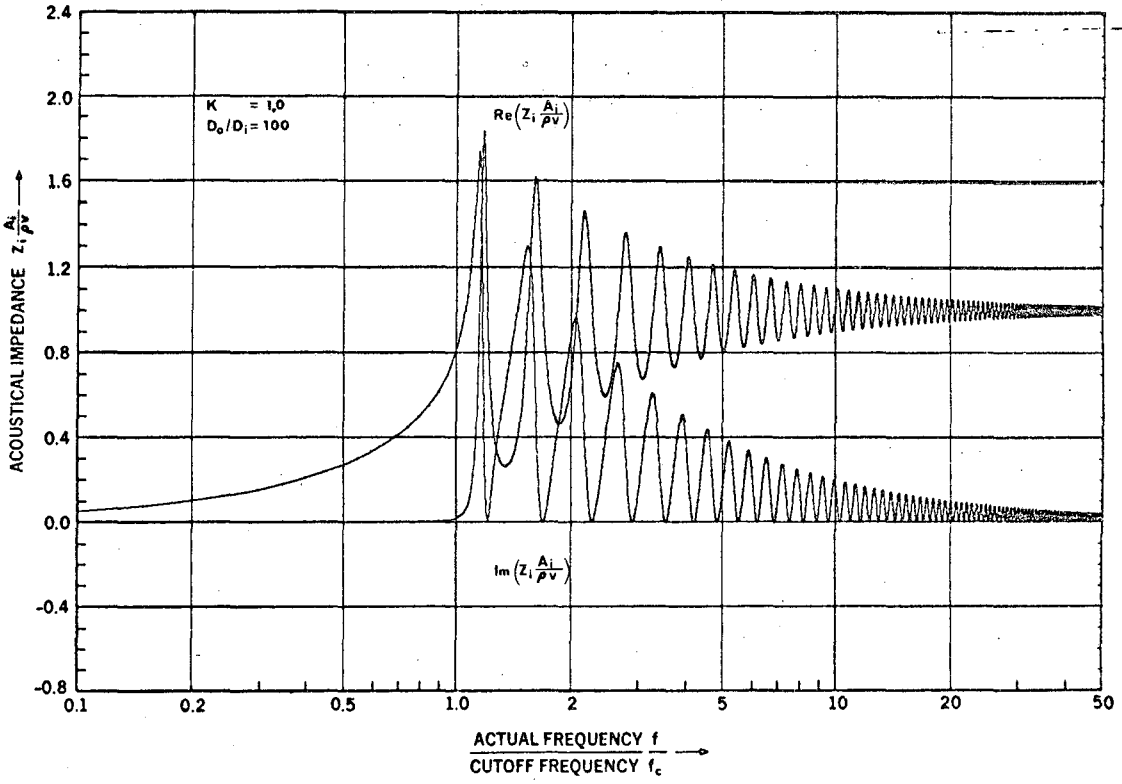

FIG. 15

XBL 674-1353

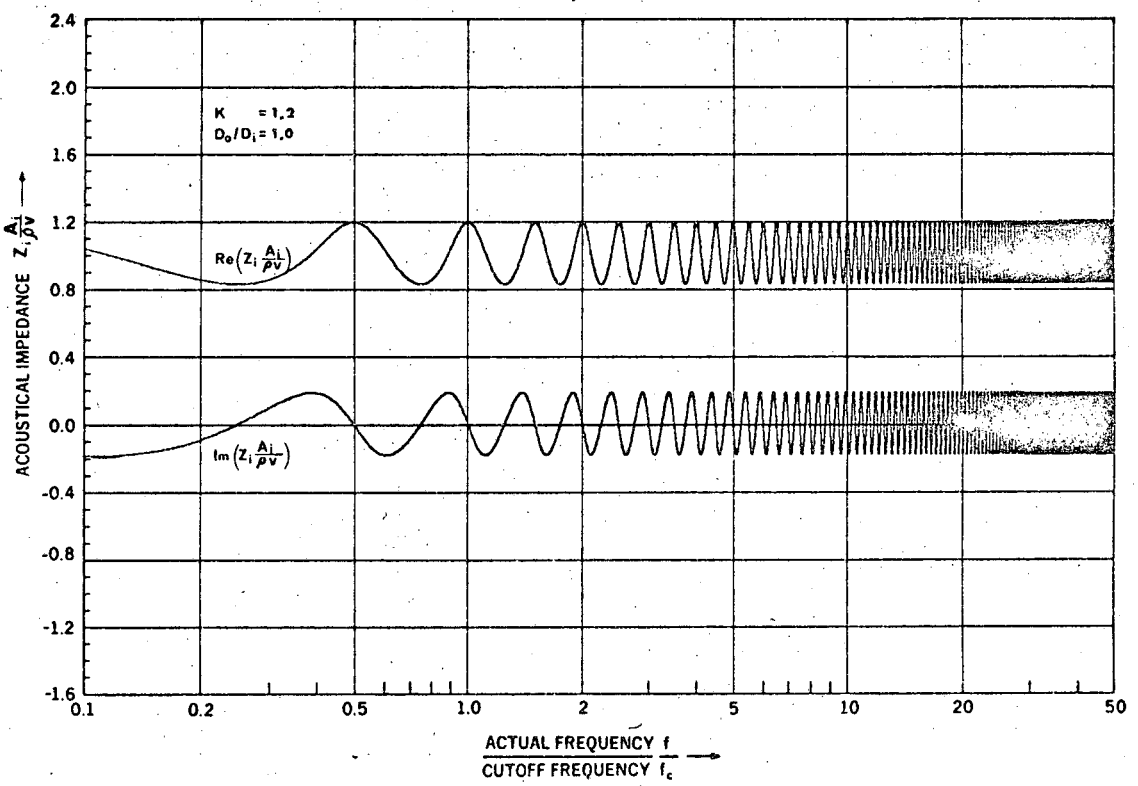

FIG.16

XBL 674-1354

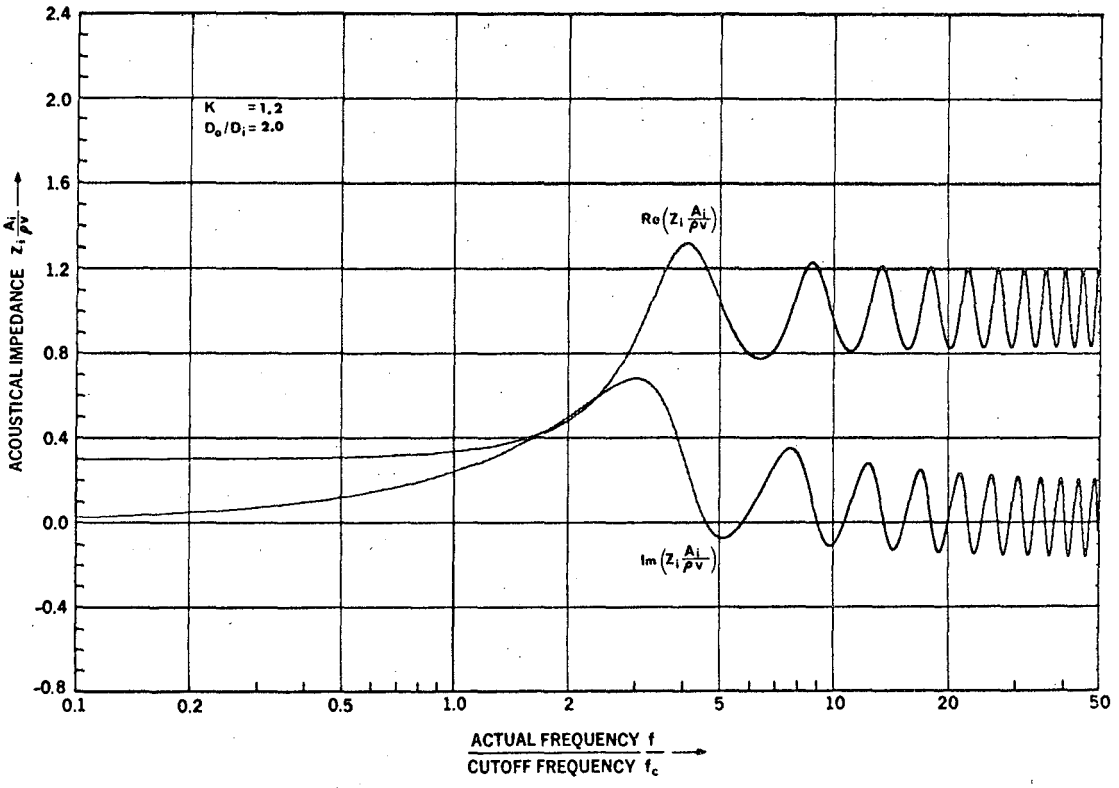

FIG.17

XBL 674-1355

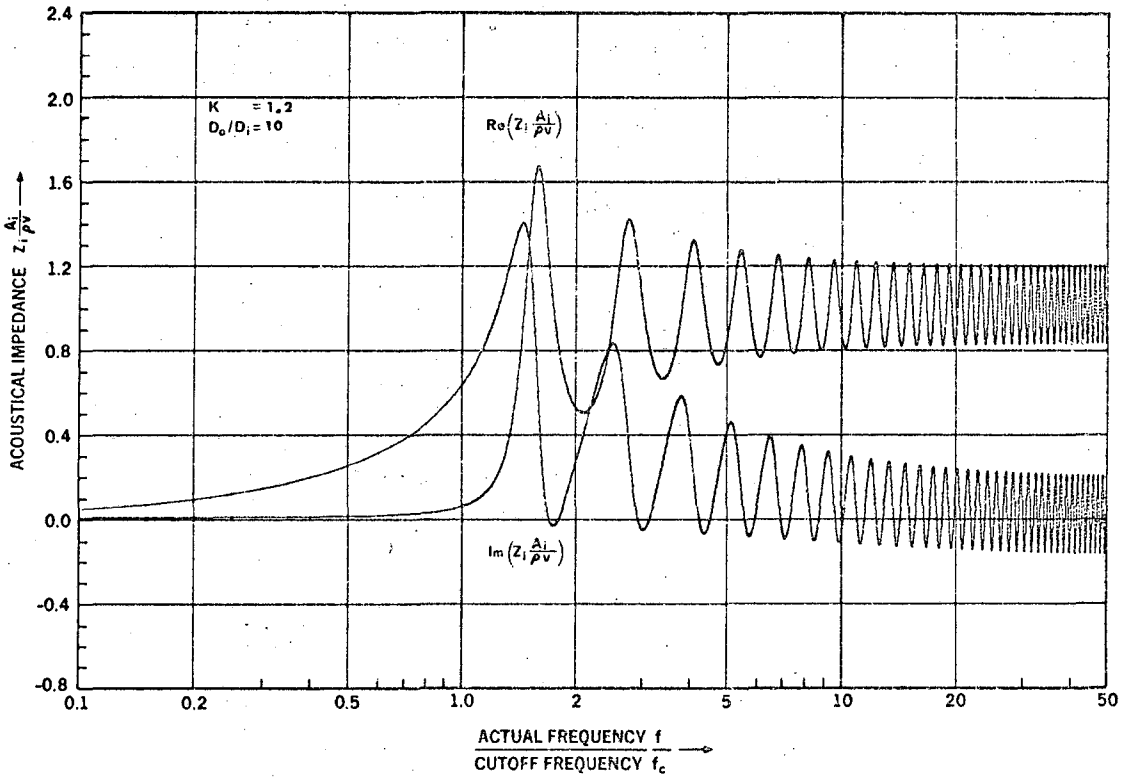

FIG.18

XBL 674-1356

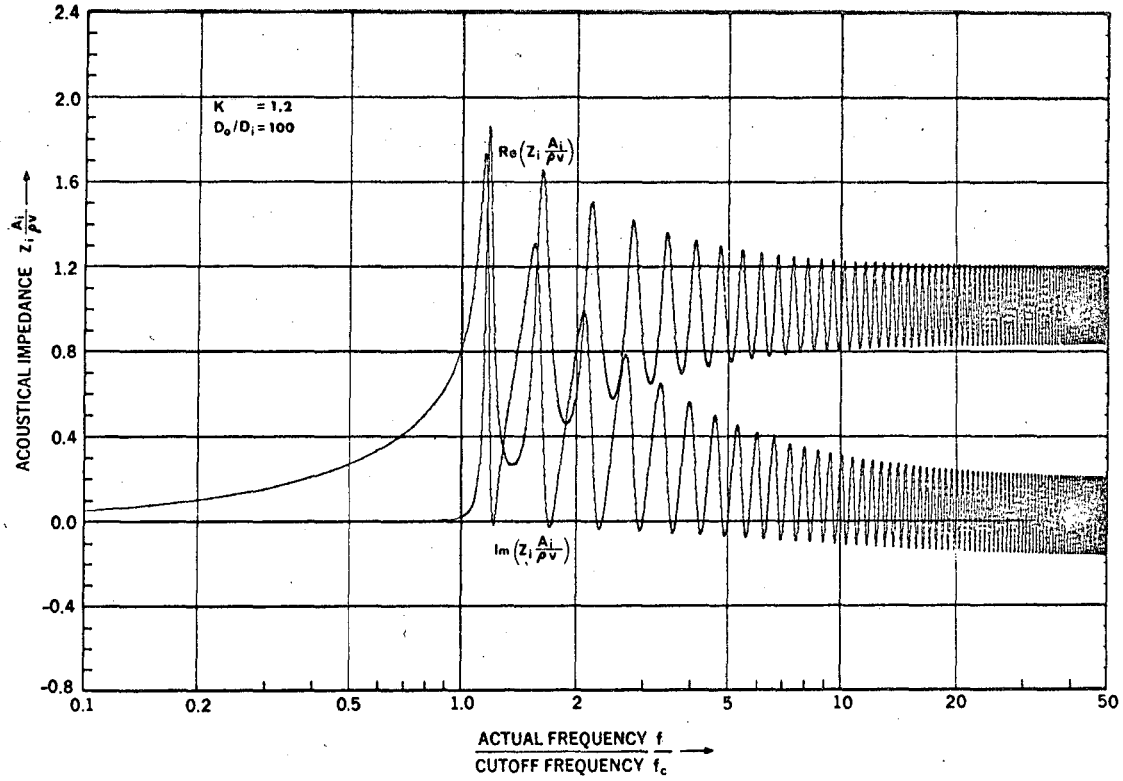

FIG.19

XBL 674-1357

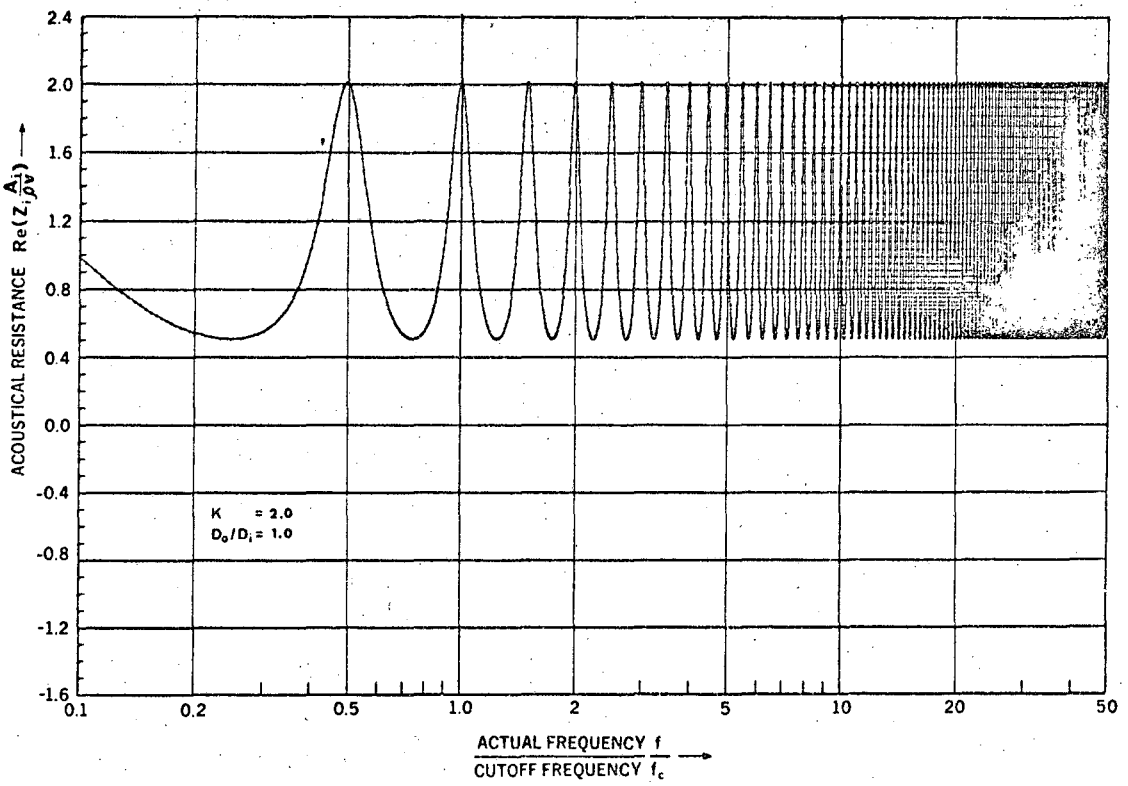

FIG. 20

XBL 674-1358

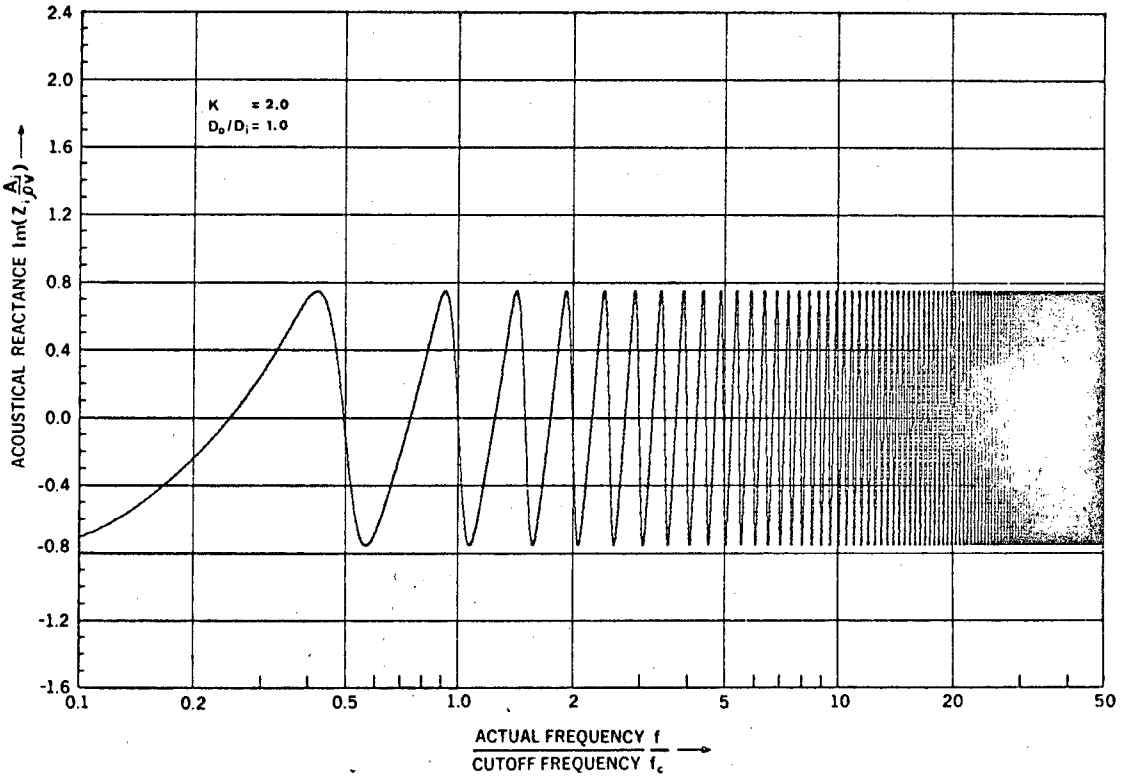

FIG. 21

XBL 674-1359

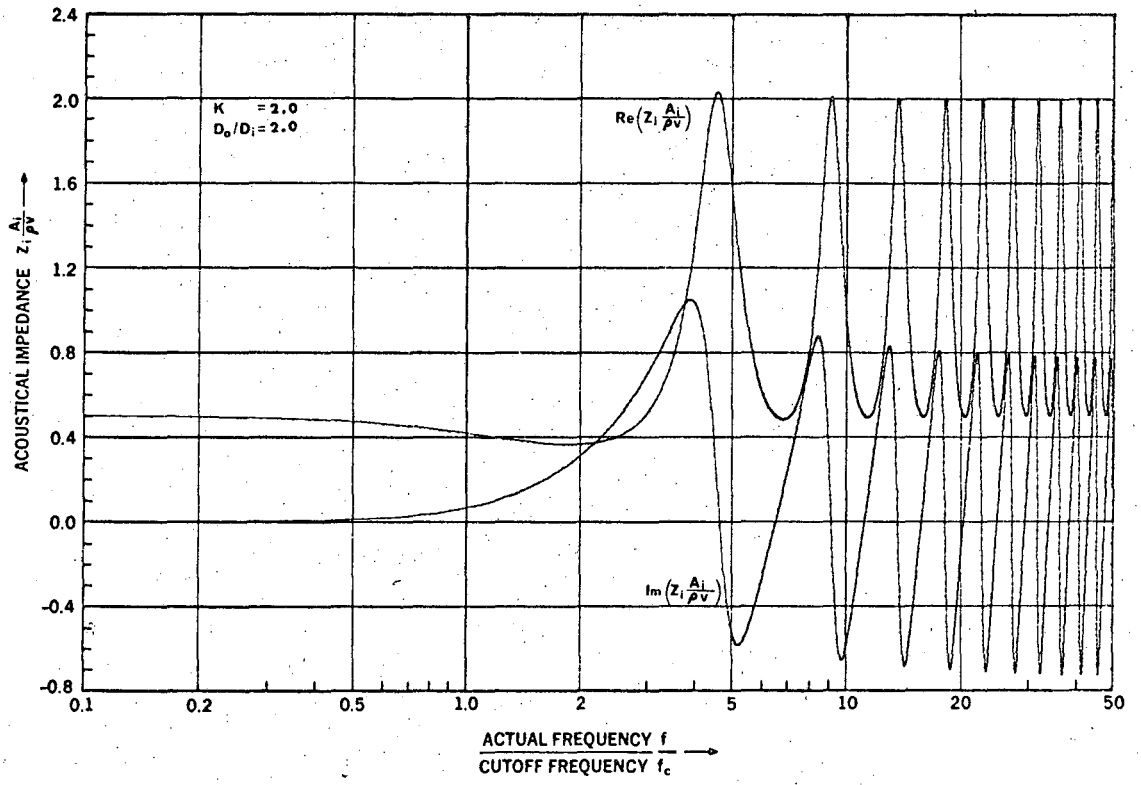

FIG. 22

XBL 674-1360

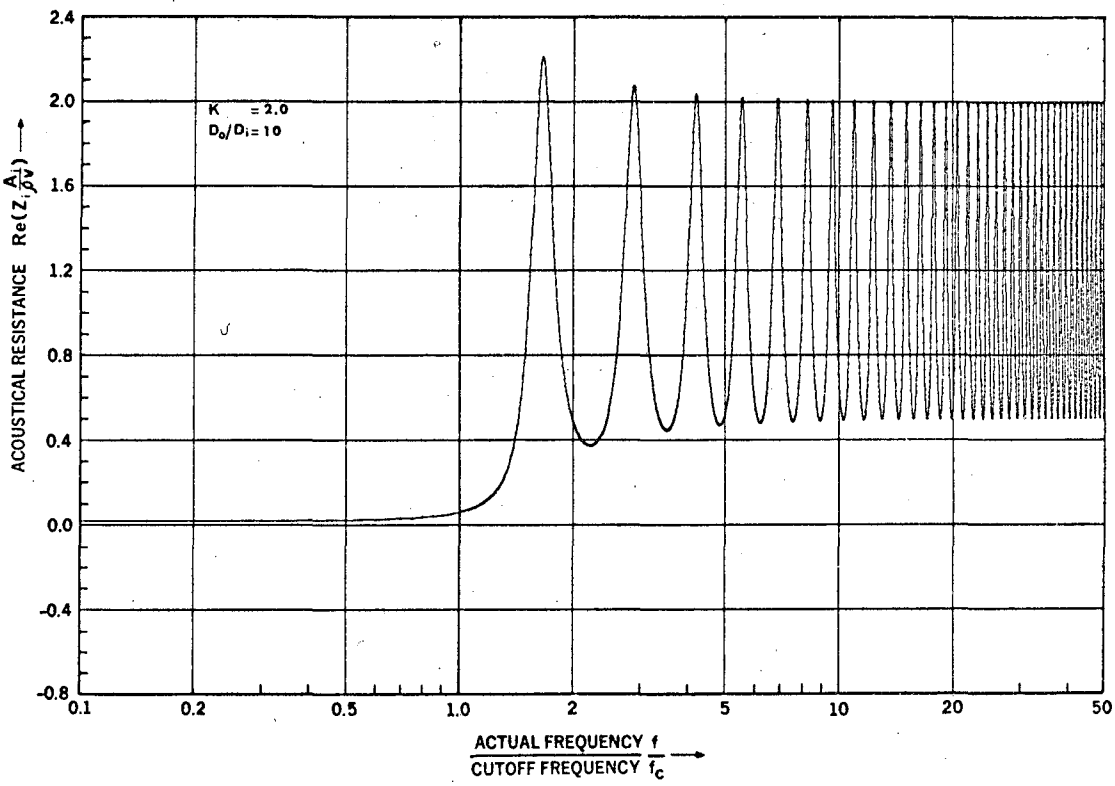

FIG. 23

XBL 674-1361

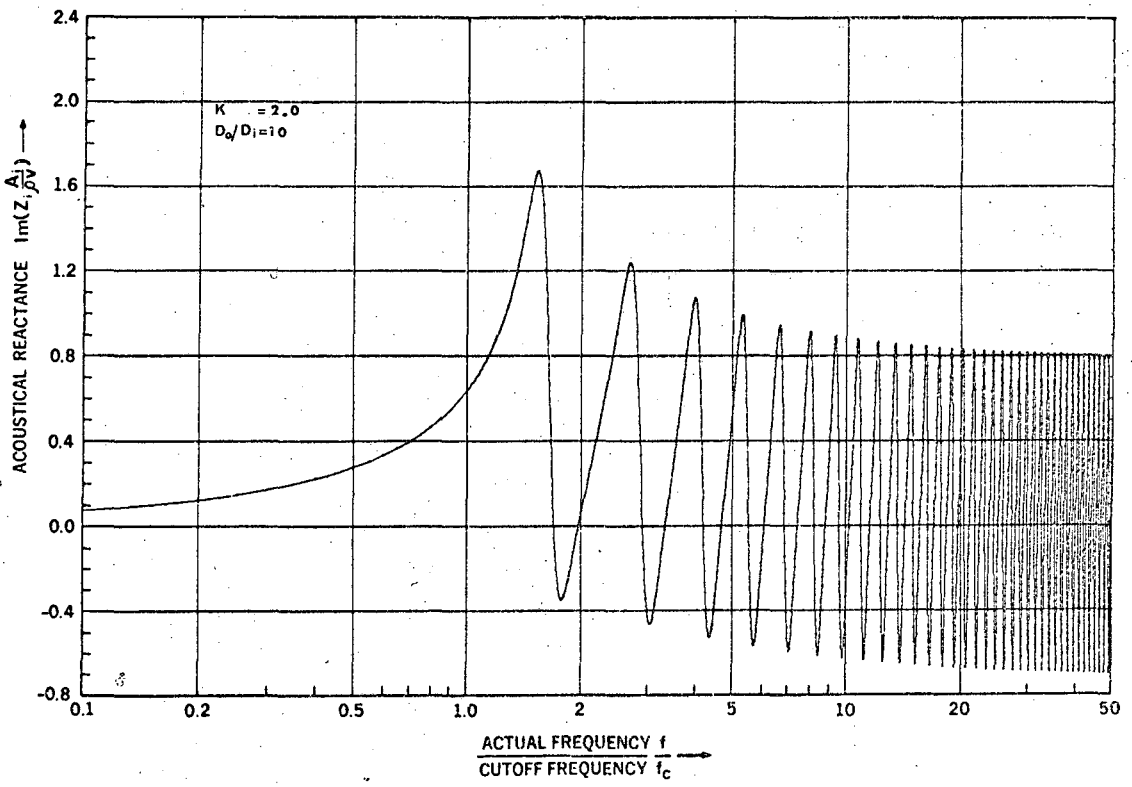

FIG. 24

XBL 674-1362

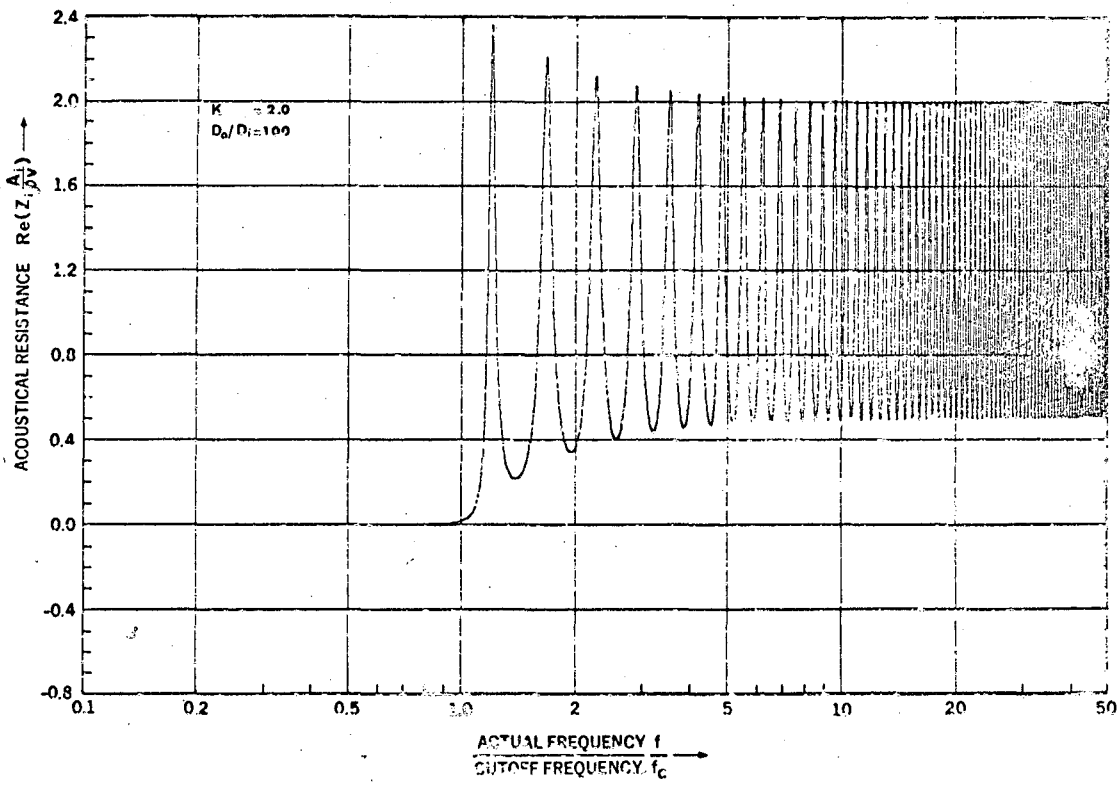

FIG. 25

XBL 674-1363

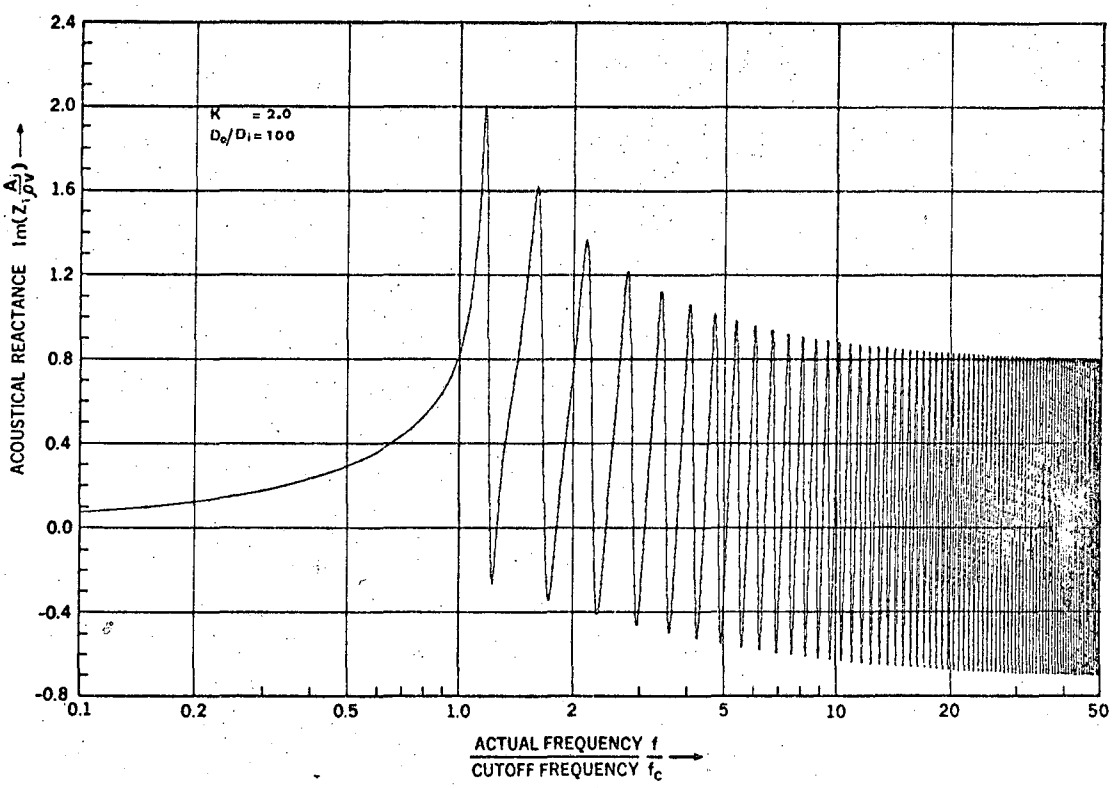

FIG.26

XBL 674-1364

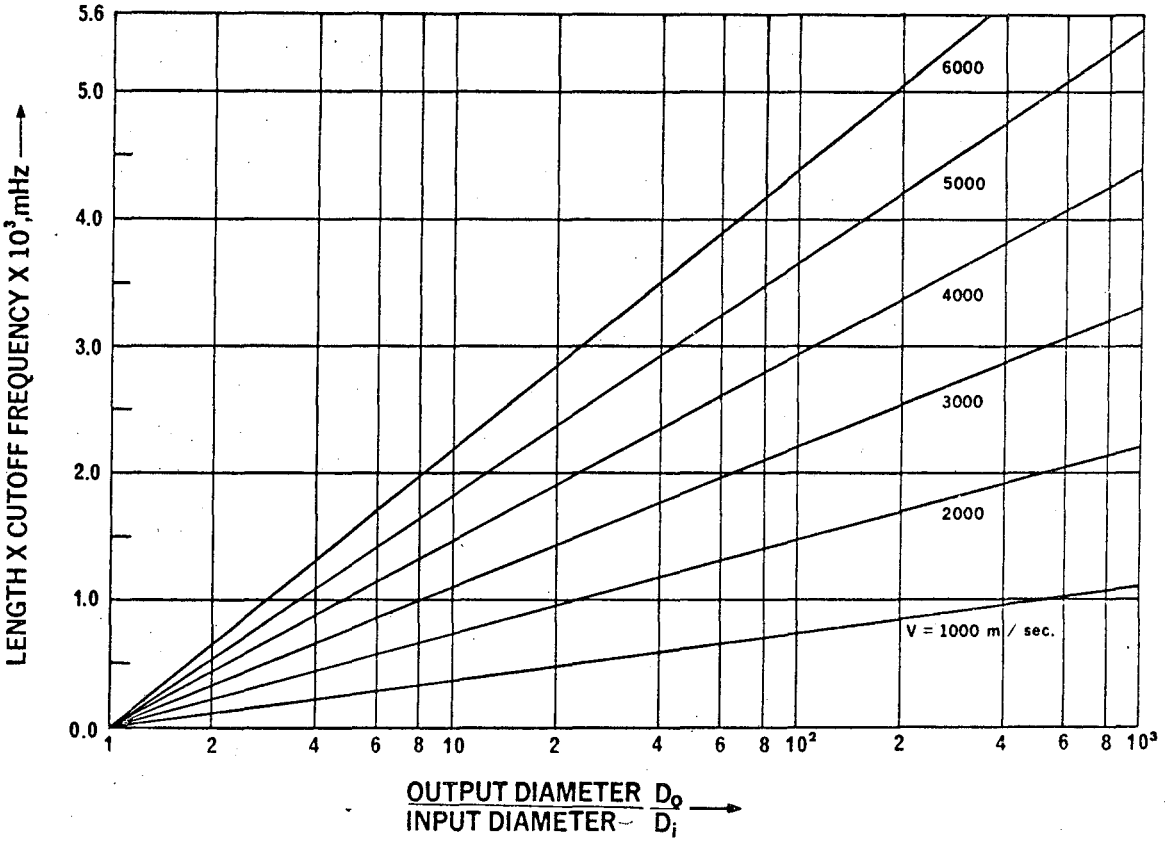

FIG. 27

XBL 674-1365